Profiling and compaction behavior of a slope-adaptive system for cross-slope no-till planting: Simulation and field insights

Hang Li[1,2], Jin He[1,2*], Huilong Chu[1], Hongwen Li[1,2], Qingjie Wang[1,2], Chao Wang[1,2], Yunpeng Li[1], Ziqing Meng[1]

(1. *College of Engineering, China Agricultural University, Beijing 100083, China*;
2. *Scientific Observing and Experiment Station of Arable Land Conservation (North Hebei), Ministry of Agricultural and Rural Affairs, Beijing 100083, China*)

Abstract: To enhance the operational stability and adaptability of soil-covering and compaction devices during no-till seeding on sloped farmland, this study developed a DEM–MBD coupled simulation model suited for conditions involving real-time slope variation and applied it to the design and analysis of a slope-adaptive covering–compacting device (SACCD). By coupling multi-body dynamics with the discrete element method, the model simulated the motion behavior and soil interaction process of the SACCD under different slope change rates, revealing its asynchronous response characteristics and profiling compaction mechanisms during dynamic slope transitions. Field experiments further verified the device's performance and the accuracy of the simulation. At the Lishu test site, the SACCD achieved a coefficient of variation of soil compaction of 20.4% under an average surface slope variation rate of 0.087 rad/s. At the Keshan test site, the coefficient of variation of soil compaction was 18.9%, with an almost constant slope. The differences between simulation and field results for the coefficient of variation of soil compaction were 8.32% (Lishu) and 1.02% (Keshan), confirming the reliability of the model and the rationality of the SACCD structural design. Overall, the simulation and field results demonstrate that the SACCD can maintain effective profiling posture and compaction performance under dynamic slope variation, providing a feasible approach and theoretical basis for the design and performance prediction of soil-covering and compaction devices for complex sloped farmland.

Keywords: variable slope, cross-slope, slope-adaptive, compaction, DEM-MBD
DOI: 10.25165/j.ijabe.20261901.10094

Citation: Li H, He J, Chu H L, Li H W, Wang Q J, Wang C, et al. Profiling and compaction behavior of a slope-adaptive system for cross-slope no-till planting: Simulation and field insights. Int J Agric & Biol Eng, 2026; 19(1): 67–75.

1 Introduction

The black soil region of Northeast China is one of the three major black soil zones in the world and serves as the main maize production area in the country. Hilly areas account for approximately one-third of the total area in Northeast China and are primarily distributed in the core regions of the black soil zone. Due to excessive tillage, this region has experienced severe soil erosion, resulting in the thinning of the black soil layer and a decline in soil organic matter, which seriously hinders sustainable agricultural development[1-3]. In these hilly areas, cross-slope planting and along-slope planting are the two common seeding approaches. Cross-slope planting has been shown to effectively prevent soil erosion and mitigate the degradation of black soil[4,5]. However, existing seeders are primarily designed for flat terrain and lack the ability to adapt to lateral surface undulations, resulting in poor covering and compacting performance on sloping farmland. Therefore, designing suitable covering-compacting devices for seeders operating in the hilly regions of Northeast China is of great importance.

The performance of covering-compacting devices largely depends on their adaptability to uneven terrain. By precisely regulating the compaction force applied to the soil surface, a consistent pressure can be maintained, which helps to prevent uneven seedling emergence. Excessive compaction may cause soil hardening and negatively affect crop emergence, while insufficient pressure can lead to poor contact between seeds and soil, impairing water absorption[6-9]. Most existing studies on covering-compacting devices focus on improving pressure control on flat terrain. For example, Sharipov et al.[10,11] mounted multiple sensors on the seeder frame to measure field surface profiles in real time, thereby improving the ground-following performance of the press wheels and enhancing seed depth consistency. Cao et al.[12] designed a pneumatic pressure control system based on air springs to address uneven furrow compaction in no-till seeders, which improved the stability of field compaction. However, relatively few studies have explored covering-compacting devices specifically for hilly terrain. To improve adaptability to undulating surfaces, such devices must be capable of both lateral and longitudinal ground following. For example, due to the shallow seeding depth required in dry direct-seeding of rice, even minor surface undulations can result in significant variability in seeding depth, affecting emergence rates.

Received date: 2025-08-12 **Accepted date:** 2025-12-09
Biographies: Hang Li, PhD candidate, research interest: conservation tillage and equipment, Email: hli@cau.edu.cn; **Huilong Chu**, BS candidate, research interest: conservation tillage and equipment, Email: chuhuilong1022@outlook.com; **Hongwen Li**, PhD, Professor, research interest: conservation tillage and equipment, Email: lhwen@cau.edu.cn; **Qingjie Wang**, PhD, Professor, research interest: conservation tillage and equipment, Email: wangqingjie@cau.edu.cn; **Chao Wang**, PhD, Associate Professor, research interest: conservation tillage and equipment, Email: superc@cau.edu.cn; **Yunpeng Li**, BS candidate, research interest: conservation tillage and equipment, Email: liyunpeng44298@outlook.com; **Ziqing Meng**, BS candidate, research interest: conservation tillage and equipment, Email: GraciaUA8389@outlook.com.
***Corresponding author: Jin He**, PhD, Professor, research interest: conservation tillage and equipment. College of Engineering, China Agriculture University, No.17 Qinghua East Road, Haidian District, Beijing 100083, China. Tel: +86-10-62737300, Email: hejin@cau.edu.cn.

To address this issue, Zhang et al.[13] developed a bidirectional micro-profiling compaction device that effectively improved seedling emergence in rice dry-seeding operations. Jia et al.[14] designed a bidirectional contour-following elastic roller that enhanced the stability of soybean seeding on ridged terrain, improving seedling emergence rate and uniformity.

To determine the optimal operating parameters and improve performance, it is necessary to analyze the interaction between agricultural machinery and soil. Traditional soil bin and field experiments can only provide macroscopic insights into soil disturbance and are inadequate for observing tool–soil interactions at the contact level. As a result, Discrete Element Model (DEM) has become widely recognized as an effective approach for simulating soil–tool interactions, particularly in exploring the micro-mechanical responses between agricultural tools and soil particles[15]. Prior studies have used DEM to analyze dynamic soil compaction[16], investigate soil deformation mechanisms inspired by bionic structures[17], and evaluate how blade geometry affects torque and soil disturbance[18]. These studies demonstrate the value of DEM in revealing particle-scale behavior; however, they primarily focus on isolated tool–soil interactions and do not capture the system-level mechanical behavior of complex agricultural machinery. Because DEM alone cannot model the internal mechanical constraints and motion relationships within multi-body equipment[19,20], Multi-Body Dynamics (MBD) is often introduced to analyze mechanical system kinematics and dynamics[21,22]. The integration of DEM and MBD has therefore emerged as an effective strategy for enhancing simulation realism, particularly when tool motion and soil responses are strongly coupled. Recent studies have successfully applied DEM–MBD coupling to analyze cleaning performance of straw-removal devices[23], soil–film–tooth interaction mechanisms[24], and seed delivery behavior within planting assemblies[25]. Nevertheless, these applications mainly focus on machinery operating under relatively stable or single-direction disturbance conditions. A critical gap remains in understanding soil–machine interactions when machinery operates under dynamically changing slope conditions, where gravitational components, profiling behavior, and force transmission become significantly more complex. Addressing this gap is essential for improving the performance of soil-covering and compaction devices on sloped farmland.

These studies have provided the necessary tools and theoretical foundations for analyzing the operation of covering-compacting devices on cross-slopes. However, few have addressed the dynamic response of such devices under real-time slope variation, which limits their applicability in complex hilly terrain. In this study, a novel DEM-MBD coupled simulation model was constructed to account for dynamic slope variation. By introducing the slope change rate—defined as the variation in terrain inclination per second of machine forward movement—as a parameter, the model simulated the operation of the SACCD on non-static terrain and revealed the asynchronous response mechanism of the wheel group and its effect on compaction performance. Furthermore, key structural parameters were optimized using response surface methodology, and the simulation model was validated through field experiments. The results demonstrated a high degree of agreement between simulation and field data, significantly improving the model's reliability and engineering applicability. This research offers new insights and technical pathways for intelligent design and performance prediction of agricultural machinery in hilly landscapes.

2 Materials and methods

2.1 Theoretical analysis of the slope-adaptive covering-compacting device

A tractor tows a no-till planter to perform cross-slope no-till seeding operations on sloping farmland. During such operations, the soil surface typically exhibits significant lateral undulations and complex micro-topography due to natural terrain variation and prior tillage patterns. These undulations can lead to uneven soil covering and inconsistent compaction if the compacting mechanism lacks sufficient adaptability. To address this challenge, a SACCD was developed to improve the operational stability and soil contact performance of the planter under dynamic slope conditions. As shown in Figure 1, the SACCD consists of two independently suspended covering-compacting wheels, each coupled with a dedicated spring-damper mechanism. This configuration enables each wheel to respond individually to variations in ground elevation. The spring assemblies provide vertical compliance, allowing the wheels to maintain continuous contact with the soil surface even in the presence of abrupt lateral slope changes. The damping characteristics further reduce excessive vibrations, promoting stable pressure transmission during motion. When the terrain exhibits large lateral undulations, the SACCD design ensures that both wheels can adjust their positions autonomously, distributing compaction force more uniformly across the furrow zone. This adaptive mechanism enhances soil coverage over the seed row and improves the compaction uniformity, which are critical factors influencing seed-soil contact, moisture retention, and subsequent seedling emergence. The implementation of SACCD thus contributes to better seeding quality and agronomic performance under variable terrain conditions.

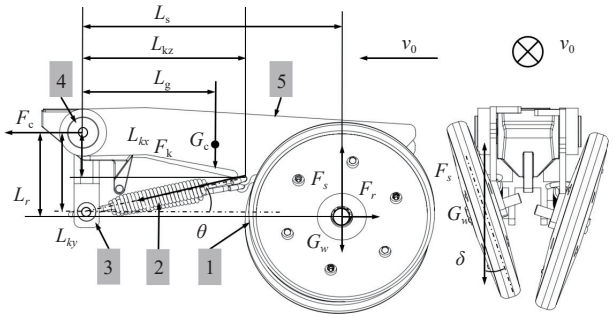

1. Covering-compacting wheel; 2. Spring; 3. Support frame; 4. Rotating frame; 5. Connecting plate. F_c: Traction force exerted by the seeding unit on the SACCD (N); G_c: Gravity acting on the connecting plate (N); F_k: Spring force acting on the wheel (N); G_w: Gravity on the wheel (N); F_s: Compaction force (N); F_r: Resistance from the ground acting on the wheel (N); L_s: Horizontal distance between the wheel axle and the rotating frame axis (m); L_{ky}: Vertical distance between the two hinge points connecting the spring and the connecting plate (m); L_{kz}: Horizontal distance from the spring-connecting plate hinge to the rotating frame axis (m); L_g: Horizontal distance from the center of gravity of the connecting plate to the rotating frame axis (m); L_r: Vertical distance from the wheel axle to the rotating frame axis (m); L_{kx}: Vertical distance from the spring-connecting plate hinge to the rotating frame axis (m); θ: Angle between the spring axis and the horizontal plane (°); v_0: Forward speed of the SACCD (m/s); δ: The inclination angle of the covering–compacting wheel relative to the ground (°).

Figure 1 SACCD structural composition and force analysis

The main structural components of SACCD are shown in Figure 1. The mechanical properties of the spring directly affect the stability of the compaction force. To determine the relationship between the spring's output force and the compaction force, a force

analysis was conducted on SACCD. During operation, SACCD performs bidirectional profiling along the undulating seedbed surface, and the magnitude of the compaction force applied by the wheel to the soil is primarily determined by the force the spring exerts on the connecting plate.

The horizontal component of the spring's output force is counteracted by the reaction force from the support frame. The vertical component of the spring force is the primary factor affecting the compaction force. Taking the axis of the rotating frame as the rotational center, the moment equilibrium equation can be derived as:

$$F_s = \frac{G_c L_g + F_k L_{kz} \sin\theta + F_k L_{kx} \cos\theta + G_w L_s - F_r L_r}{L_s} \quad (1)$$

When the surface undulation is Δx, the variation in spring force ΔF_k can be expressed as:

$$\Delta F_k = \frac{k L_{kz} \Delta x}{L_s \sin\theta} \quad (2)$$

From Figure 1 and Equation 1, it can be seen that once the installation positions of SACCD components are fixed, the variations in parameters such as $G_c L_g$, $G_w L_s$, L_{kz}, and θ remain minimal as the surface undulation Δx changes. In this case, ΔL_{kz} is negligible, and ΔL_{kx} and ΔL_r can be approximated by Δx. Thus, the variation in compaction force can be approximated as:

$$\Delta F_s = \frac{k F_k L_{kz}^2 \Delta x}{L_s^2} + \frac{F_k \Delta x \cos\theta - \Delta F_r \Delta x}{L_s} \quad (3)$$

From the above analysis, it is concluded that the fluctuation ΔF_s in compaction force due to surface undulation Δx is mainly influenced by ΔF_r, L_{kz}, L_s, k, F_k, and θ. Here, ΔF_r is the variation in ground resistance, which depends on both the physical-chemistry properties of the soil and the terrain profile. Larger L_{kz} results in greater ΔF_s, while a larger L_s reduces ΔF_s. Greater spring stiffness k also increases ΔF_s. The magnitude of F_k affects both k and ΔF_s, and is determined by the spring's extension length and stiffness k, which should be selected based on the soil properties and agronomic requirements for seeding. According to field conditions for no-till seeding on sloped farmland in Northeast China, k=10 N/mm is adopted[12,13,26]. Therefore, the primary factors influencing ΔF_s are L_{kz} and L_s. Although increasing L_s reduces the compaction force fluctuation, an overly long L_s increases the distance between the compaction unit and the furrow opener, potentially affecting seeding quality during cross-slope strip seeding due to slope variation. As shown in Figure 1, the value of L_s also constrains the maximum allowable value of L_{kz}, making the design of L_s dependent on L_{kz}.

The soil compression force F_{cr} applied by the wheel can be expressed as:

$$F_{cr} = (F_k \sin\theta + G_w)\cos\delta \quad (4)$$

From Equation 4, the main parameters affecting soil covering and compaction effectiveness are θ and δ. Here, θ is the angle between the spring axis and the horizontal plane. As per Equation 3, larger θ values correspond to smaller ΔF_s. The value of θ is determined by L_{ky} and L_{kz}. In conclusion, the key parameters influencing the fluctuation ΔF_s of SACCD's compaction force are L_{ky}, L_{kz}, and δ.

2.2 DEM-MBD coupled simulation model

The Edinburgh Elasto-Plastic Adhesion (EEPA) model can effectively simulate the variation in inter-particle contact forces of non-linear elastic soils during compression, demonstrating notable advantages in modeling the compaction behavior of black soils in Northeast China[13,26]. In order to establish a simulation framework capable of accurately predicting the operational performance of the SACCD under conditions of dynamically varying terrain gradients, this study adopted intrinsic parameters of soil and steel from relevant literature[27-29]. In previous work, based on the physical properties of soil samples collected from the field, the contact parameters between soil-soil and soil-steel were calibrated using the angle of repose method. The EEPA model parameters were further calibrated through the flat-plate compression test and the cone penetration test (Table 1)[26].

Table 1 Simulation parameters based on EEPA model

Parameter	Value
Steel density/kg·m^{-3}	7860
Shear modulus/Pa	7.94e+10
Poisson's ratio	0.28
Soil Poisson's ratio	0.25
Soil shear modulus/Pa	5e + 07
Soil density particle/kg·m^{-3}	2670
Constant pull-off force/N	0
Surface energy/J·m^{-2}	76
Contact plasticity ratio	0.3
Slope exponent	1.5
Tensile exponent	2.69
Tangential stiff multiplier/N·m^{-1}	0.59
Restitution coefficient: Soil-Soil	0.51
Static friction coefficient: Soil-Soil	0.63
Rolling friction coefficient: Soil-Soil	0.34
Restitution coefficient: Soil-Steel	0.56
Static friction coefficient: Soil-Steel	0.58
Rolling friction coefficient: Soil-Steel	0.44

During transverse slope operations in the field, the gradient of the terrain changes in real time, making it challenging to construct a soil particle model that dynamically reflects such changes. To simulate the real-time variation of surface slope encountered by the SACCD, this study employed a DEM-MBD coupled simulation approach. The SACCD was rotated relative to the soil particles to emulate the change in operating slope during transverse field operations (Figure 2). To achieve this, the SACCD and furrow opener were first constrained in RecurDyn V9R2 (FunctionBay, Seoul, South Korea) using Fixed, Translate, Revolute, Spring, and GeoSur settings to appropriately restrict the degrees of freedom. Subsequently, a rotational velocity relative to the soil particles was applied to both components to simulate the real-time variation of terrain slope. Finally, the SACCD and furrow opener models were exported in Wall file format and imported into EDEM 2020, establishing a data transmission interface for DEM-MBD coupling between RecurDyn V9R2 and EDEM 2020 (Altair Engineering, Troy, Michigan, USA).

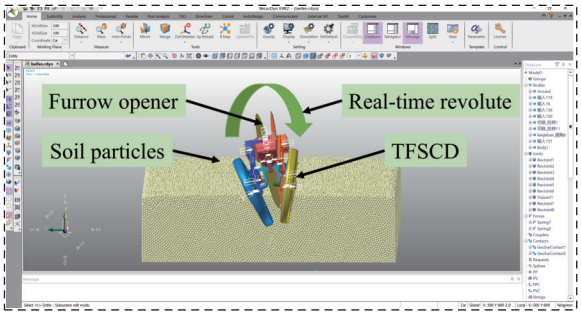

Figure 2 Real-time variation process of SACCD in response to surface slope changes

2.3 Simulation test methods

The simulation tests were divided into two categories: optimization tests and comparative tests. The objective of the optimization simulation tests was to evaluate the effects of different SACCD design parameters on seedbed uniformity and to optimize the key operational parameters of the SACCD. Soil compaction, primarily determined by the reshaping capacity of the covering-compacting device on furrowed soil, is an important indicator of operational quality and a direct physical measure of SACCD performance[13,16,30,31]. In this study, an orthogonal experimental design was adopted using L_{ky}, L_{kz}, and δ as test factors and the coefficient of variation in soil compaction (CVSC) as the evaluation metric (Table 2).

Table 2 Experimental factors used in the orthogonal optimization

Test code	Test factors		
	L_{ky}/mm	L_{kz}/mm	δ/(°)
–1.682	100	220	10
–1	110	228	12
0	125	240	15
1	140	252	18
+1.682	150	260	20

The comparative simulation tests aimed to investigate the effect of different real-time slope variation rates on SACCD performance under optimal operational parameters. The slope variation rate was set as the experimental factor, and CVSC was again used as the evaluation metric. In the experimental site located in Lishu County in Jilin Province (124°97′E, 43°18′N), terrain slope measurements revealed a maximum slope change of approximately 12.5° over a 5 m horizontal distance. Based on these field measurements and the forward velocity of the machine, the maximum real-time slope variation rate was calculated to be approximately 0.175 rad/s. Therefore, a single-factor test was designed with five slope variation rates: 0, 0.087, 0.175, 0.262, and 0.350 rad/s.

2.4 Field experiment validation

To validate the operational performance of the SACCD and the accuracy of the simulation model, a prototype was fabricated based on the optimized parameters obtained from the simulations. Field tests were conducted at two experimental sites (Figure 3): Lishu County in Jilin Province (124°97′E, 43°18′N) and Keshan County in Heilongjiang Province (125°50′E, 48°1′N). Both sites are located in the black soil hilly region of Northeast China, where the cropping system is characterized by annual no-till transverse slope sowing of maize. At the Lishu site, the surface straw coverage was measured at 0.71 kg/m^2. At the Keshan site, straw was managed through row-return practices, with coverage at 1.48 kg/m^2 and a straw clearance rate of 93.6% in the seeding zone after treatment. The forward velocity of the no-till planter was maintained at 2 m/s, consistent with the simulation setup. A soil compaction tester was used with a five-point sampling method to evaluate SACCD performance after sowing. The measurement depth was 0-100 mm, and the insertion speed of the compaction tester was approximately 10 mm/s[26]. Additionally, the seeding depth stability was assessed using the same five-point sampling method.

3 Results and discussion

3.1 Analysis of SACCD operation process

A simulation of the SACCD operation process was conducted under a terrain slope variation rate of 0.350 rad/s. The simulation

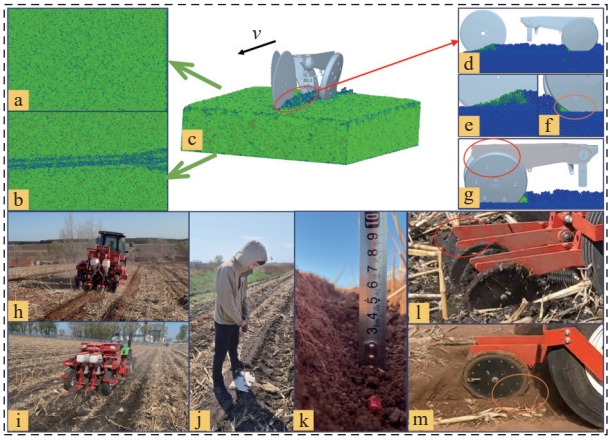

a. Soil particle surface before SACCD operation; b. Soil particle surface after SACCD operation; c. Schematic diagram of SACCD and furrow opener operation; d. Schematic representation of soil particle movement during SACCD and furrow opener operation; e. Schematic representation of soil particle movement during furrow opener operation; f. Schematic representation of soil particle movement during SACCD operation; g. Simulation result showing the profiling performance of SACCD; h. Field operation of SACCD in Lishu County; i. Field operation of SACCD in Keshan County; j. Soil compaction measurement. k. Seeding depth measurement; l. Field profiling performance of SACCD; m. Soil-SACCD interaction during field operation.

Figure 3 Comparison and analysis of field operations and simulation process

scenario, where the SACCD maintains stable contact with the soil surface, is illustrated in Figure 4. To mimic the real-time variation in terrain slope during field operation, the SACCD was subjected to continuous rotational adjustment relative to the soil particle bed. Since the SACCD must engage with the soil after the furrow opener has operated, rotation relative to the soil commences prior to actual soil contact. Given a rightward rotational velocity of 0.350 rad/s relative to the soil particles, an initial leftward rotational offset of 0.175 rad was applied before soil contact. At t = 0.7 s, the SACCD stably enters the post-furrowing soil region. At this point, the relative deflection angle of the SACCD and furrow opener with respect to the soil is φ = 4°. Between t = 0.8 s and t = 0.9 s, the SACCD and furrow opener continue to deflect at a rotational speed of 0.350 rad/s, emulating the real-time terrain slope variation. At t = 1.0 s, the furrow opener exits the soil, while the SACCD continues its rotational motion from t = 1.0 s to t = 1.2 s before gradually disengaging from the soil bed.

Compared with conventional covering-compacting designs commonly used in seeders for sloping farmland, the present study introduces a novel approach by integrating real-time slope variation into a DEM-MBD coupled simulation framework[13,26]. This dynamic modeling strategy enables a more realistic representation of the mechanical-soil interaction under non-uniform terrain conditions, offering deeper insights into the operational behavior of the SACCD during cross-slope no-till seeding. As illustrated in Figure 4, when the terrain undergoes lateral slope changes, the furrow opener and the SACCD rotate around a pivot point located above the support frame. This rotational movement results in a lateral shift of the furrow opener toward the left side relative to the direction of travel. Furthermore, due to the fore-aft spatial separation between the furrow opener and the SACCD, a misalignment occurs whereby the compacting wheels are no longer positioned directly above the furrow center formed by the opener. Such a misalignment can lead to reduced coverage uniformity and soil-seed contact quality. To

address this issue, the SACCD is equipped with independently suspended profiling wheels, each capable of vertical displacement in response to localized terrain undulations. This design feature partially compensates for the lateral offset and enables each wheel to maintain close conformity with the seedbed surface. Nonetheless, as the slope variation rate increases—particularly in areas with abrupt or continuous slope transitions—the SACCD's ability to maintain optimal alignment diminishes. Under these conditions, the compacting wheels may inadvertently apply pressure directly onto the furrow, which can disrupt the seed placement and reduce the effectiveness of soil covering and compaction. Such outcomes not only compromise seeding depth consistency but also increase the risk of soil crusting and seedling emergence issues. By improving the responsiveness of the profiling mechanism and minimizing lateral force deviations, the device can better accommodate terrain-induced misalignments and maintain effective compaction performance under variable slope conditions.

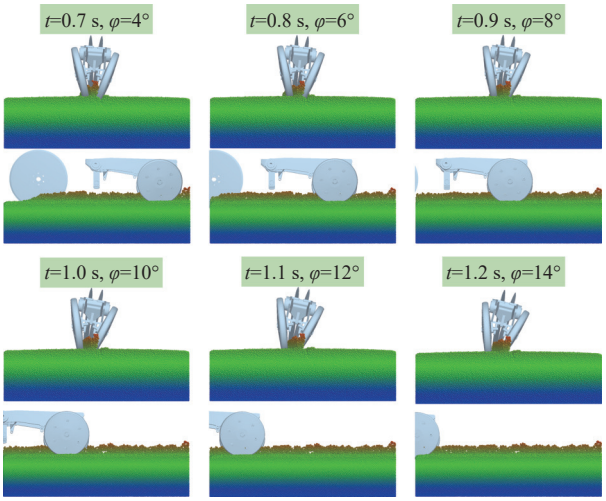

Figure 4 Analysis of the covering and compacting process under real-time slope variation conditions

Field measurements from sloping terrains in Northeast China indicated a maximum slope variation of approximately 12.5° over a 5 m horizontal distance. At an operational speed of 2 m/s, this translates to a maximum real-time slope variation rate of roughly 0.175 rad/s. The simulation in Figure 4 was conducted under a slope variation rate of 0.350 rad/s, and results demonstrated that the SACCD maintained effective soil covering and compaction performance. Therefore, the proposed SACCD design is capable of meeting the demands of real-time slope-adaptive field operations.

3.2 Optimization analysis of key SACCD parameters

The results of the simulation-based orthogonal optimization experiments are presented in Table 3. Three dimensionless coded factors were analyzed using Design-Expert 13. These correspond to the vertical distance between the spring and connecting plate joints (A), the horizontal distance from the spring-connecting plate joint to the rotating frame axis (B), and the inclination angle of the compacting wheel (C), respectively. Their influence on the CVSC was evaluated. A multivariate regression analysis was performed using Design-Expert 13, and the regression model was found to be significant ($p<0.01$). The resulting regression equation for CVSC was as follows:

$$\begin{aligned}\mathrm{CVSC} = {} & 16.87 - 1.46A - 2.32B - 5.83C + 0.2875AB + \\ & 2.14AC + 0.6875BC + 1.98A^2 + 0.3408B^2 + 3.36C^2 \end{aligned} \quad (5)$$

Optimization was conducted using the software's numerical solver, with the ranges for A, B, and C set from –1 to 1. The optimal parameter combination was identified as A = –0.14, B = 1.00, and C = 0.81, yielding a minimum predicted CVSC value of 12.89%. To visualize the relationships between the variables and CVSC, response surface plots were generated using Design-Expert 13 (Figures 5a-5f). The following trends were observed: Figures 5a, 5d (C fixed at optimum): CVSC increased with increasing B; with B fixed, CVSC first increased and then decreased with increasing A. Figures 5b, 5e (B fixed at optimum): CVSC exhibited a similar nonlinear trend with increasing A and a positive correlation with increasing C. Figures 5c, 5f (A fixed at optimum): Both B and C showed positive correlations with CVSC when the other was held constant. Based on the optimal combination, the corresponding structural parameters were determined as: L_{ky} = 122.90 mm, L_{kz} = 252.00 mm, and δ = 17.42°. For practical manufacturing, these were rounded to L_{ky} = 123 mm, L_{kz} = 252 mm, and δ = 17.5°. To validate the optimization results, a simulation test was conducted using the optimal parameter set. The resulting CVSC value was 12.08%, which closely matched the predicted value, confirming the accuracy of the regression model.

Table 3 Orthogonal experimental scheme and corresponding test results

Number	Test factors			Results
	A	B	C	CVSC/%
1	–1	–1	–1	31.2
2	1	–1	–1	28.1
3	–1	1	–1	27.6
4	1	1	–1	23.1
5	–1	–1	1	14.5
6	1	–1	1	17.4
7	–1	1	1	11.1
8	1	1	1	17.7
9	–1.682	0	0	30.7
10	1.682	0	0	17.7
11	0	–1.682	0	25.5
12	0	1.682	0	13.6
13	0	0	–1.682	37.1
14	0	0	1.682	19.1
15	0	0	0	16.0
16	0	0	0	17.4
17	0	0	0	16.5
18	0	0	0	15.3
19	0	0	0	18.7
20	0	0	0	16.7

Beyond the numerical optimization, the underlying mechanism of these parameter effects reflects the coupled interaction between wheel geometry, force transmission, and soil particle behavior under dynamic slope variation. Increasing B effectively alters the vertical lever arm of the compaction wheel, amplifying the vertical oscillation component transmitted to the soil, which explains its generally positive correlation with CVSC. Similarly, the increase in C modifies the deflection angle of the wheels, thereby influencing the partitioning of compaction forces into vertical and tangential components. This phenomenon is consistent with the soil-tool interaction patterns reported by Zhao et al.[18], who showed that changes in tool geometry can significantly affect soil compaction stability due to shifts in force direction. The nonlinear effect of A suggests that lateral support distance contributes to both the structural rigidity of the profiling mechanism and the synchronization of left–right wheel responses, echoing findings by

Xie et al.[15] and Zhang et al.[13] that lateral disturbances introduce complex particle rearrangements during dynamic soil loading. Altogether, the optimal parameter combination appears to minimize CVSC by balancing these coupled mechanical effects—reducing unnecessary lateral torque transmission, stabilizing the compaction vector, and promoting uniform soil resistance across both wheels.

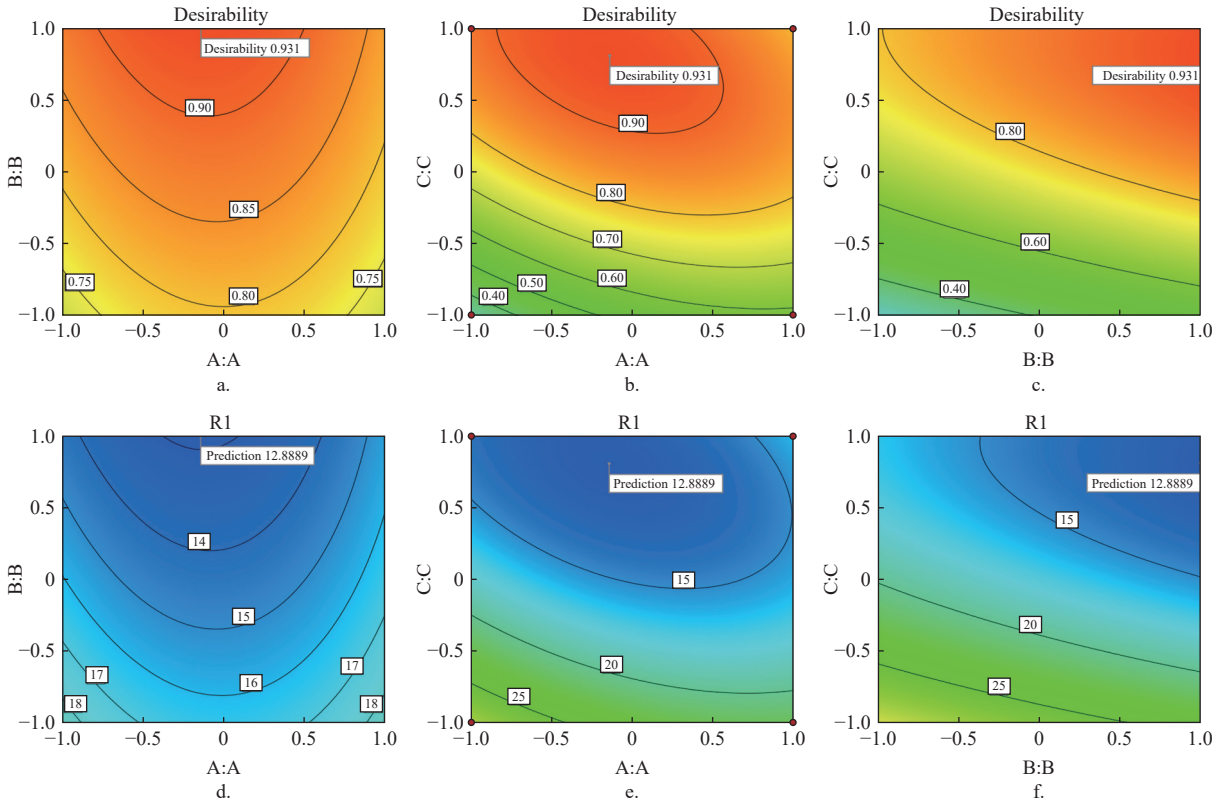

Figure 5 Response surfaces of the effects of each factor on the evaluation indices

3.3 Effect of real-time slope variation rates on the compaction stability of SACCD

To investigate the operational performance of the SACCD under different real-time slope variation rates, a single-factor simulation test was conducted with slope change rates set at 0, 0.087, 0.175, 0.262, and 0.350 rad/s. As shown in Figure 6, during the initial phase from 0 to 0.3 s, the furrow opener engaged with the soil particles for trenching, while the SACCD had not yet contacted the soil, resulting in zero compaction force. Between 0.4 and 0.6 s, the SACCD began gradually entering the soil. Due to the position of the mechanical stops, the two wheels of the SACCD were initially located slightly below the upper surface of the soil particles. When entering the soil, the side contact area between the wheels and soil particles was relatively large, causing minor bouncing due to the impact. The compaction force increased rapidly. This bouncing led to a brief drop in compaction force around 0.4-0.5 s. From 0.5 to 0.7 s, as the SACCD rebounded, it was rapidly pulled back downward by gravity and spring force, resulting in a collision with the soil particles and a sharp increase in compaction force to a peak. Between 0.7 and 1.2 s, the contact between SACCD and the soil particles stabilized, with minimal variation in compaction force, reaching a steady state. From 1.2 to 1.3 s, the SACCD gradually exited the soil, causing a rapid decrease in compaction force, which approached zero from 1.3 to 1.5 s.

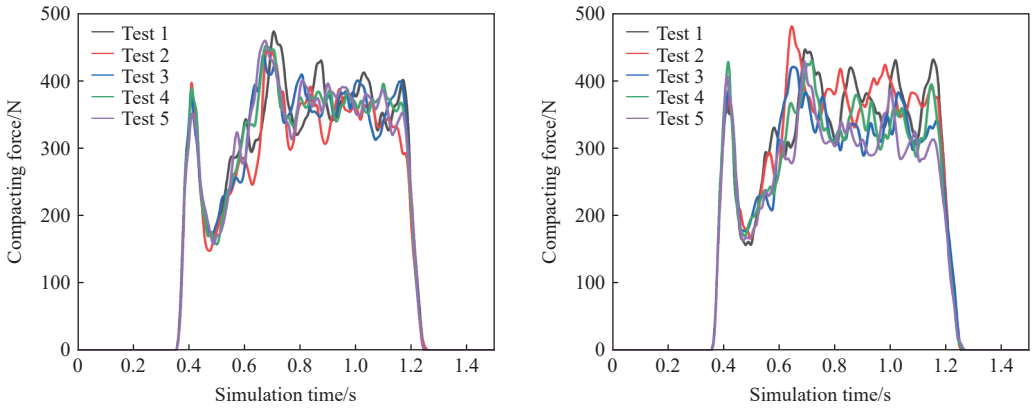

a. Left wheel compaction force curve; b. Right wheel compaction force curve; Test 1: slope variation rate = 0 rad/s; Test 2: slope variation rate = 0.087 rad/s; Test 3: slope variation rate = 0.175 rad/s; Test 4: slope variation rate = 0.262 rad/s; Test 5: slope variation rate = 0.350 rad/s.

Figure 6 Compaction force variation during SACCD operation

As shown in Figure 6, when the slope variation rate was 0 rad/s, the compaction force fluctuations of the left and right wheels were nearly identical, indicating a balanced response of the SACCD to stable terrain conditions. However, as the slope variation rate increased, a clear divergence emerged in the force responses of the two wheels: the left wheel exhibited a smaller fluctuation amplitude compared to the right wheel. This asymmetry can be primarily attributed to the inherent structural inclination of the SACCD's wheels—specifically, the left wheel is inclined toward the left, and the right wheel toward the right. During cross-slope operation, the SACCD undergoes a rotational motion toward the right in response to terrain undulations. This rotation modifies the orientation of the wheel relative to the ground surface. As the SACCD rotates rightward, the left wheel gradually assumes a more perpendicular alignment with respect to the ground, thereby increasing the proportion of the spring and gravitational forces that act directly along the vertical axis. This alignment enhances the vertical stability of the compaction force, effectively reducing its dynamic variation. In contrast, the right wheel becomes increasingly parallel to the ground surface as the SACCD continues to rotate. This altered orientation causes the resultant compaction force vector to deviate from the vertical direction, diminishing the effective vertical component of the spring force acting on the soil. As a result, the compaction force exerted by the right wheel becomes more sensitive to transient changes in terrain and structural vibration, leading to amplified fluctuations. This differential response mechanism underscores the importance of geometric alignment and real-time kinematic behavior in determining compaction uniformity under dynamically changing slope conditions. It also suggests that optimizing the wheel inclination angles or implementing adaptive mechanisms may further improve the SACCD's performance consistency on sloping farmland.

As shown in Figure 7, the spatial distribution of soil compaction following SACCD operation under various slope variation rates was visualized and quantitatively analyzed. The compaction data were obtained using a standardized soil penetrometer at incremental depths, allowing for a detailed evaluation of vertical compaction profiles. Across all test scenarios, a consistent trend was observed: the degree of soil compaction increased progressively with probe insertion depth. This phenomenon is in line with the findings reported by Xie et al.[15] and Zhang et al.[13], which demonstrated that subsurface soil layers exhibit greater resistance due to cumulative pressure and reduced soil porosity. In the black soil region of Northeast China, where the present study was conducted, the agronomic optimum seeding depth for maize is approximately 0.05 m. At this critical depth, the CVSC after SACCD operation under slope variation rates of 0, 0.087, 0.175, 0.262, and 0.350 rad·s^{-1} were 17.88%, 12.08%, 22.37%, 11.60%, and 15.46%, respectively. These values reflect the SACCD's ability to maintain compaction uniformity under varying terrain dynamics. Nevertheless, all CVSC values remain below 25%, indicating acceptable operational performance. When compared to the results reported by Zhang et al.[13], the CVSC values in this study appear relatively higher. This discrepancy is attributable to two main factors. First, the SACCD operates immediately after the furrow opener, which disturbs the soil and alters its compaction characteristics, particularly in the seeding zone. Second, the compaction apparatus[13] was developed for shallow seeding applications in dry direct-seeded rice systems, where soil surface conditions are relatively stable and micro-profiling is emphasized. In contrast, the SACCD in the current study is specifically designed to accommodate deep seeding of maize under conditions of real-time slope variation, which introduces greater terrain-induced variability and complexity into the compaction process.

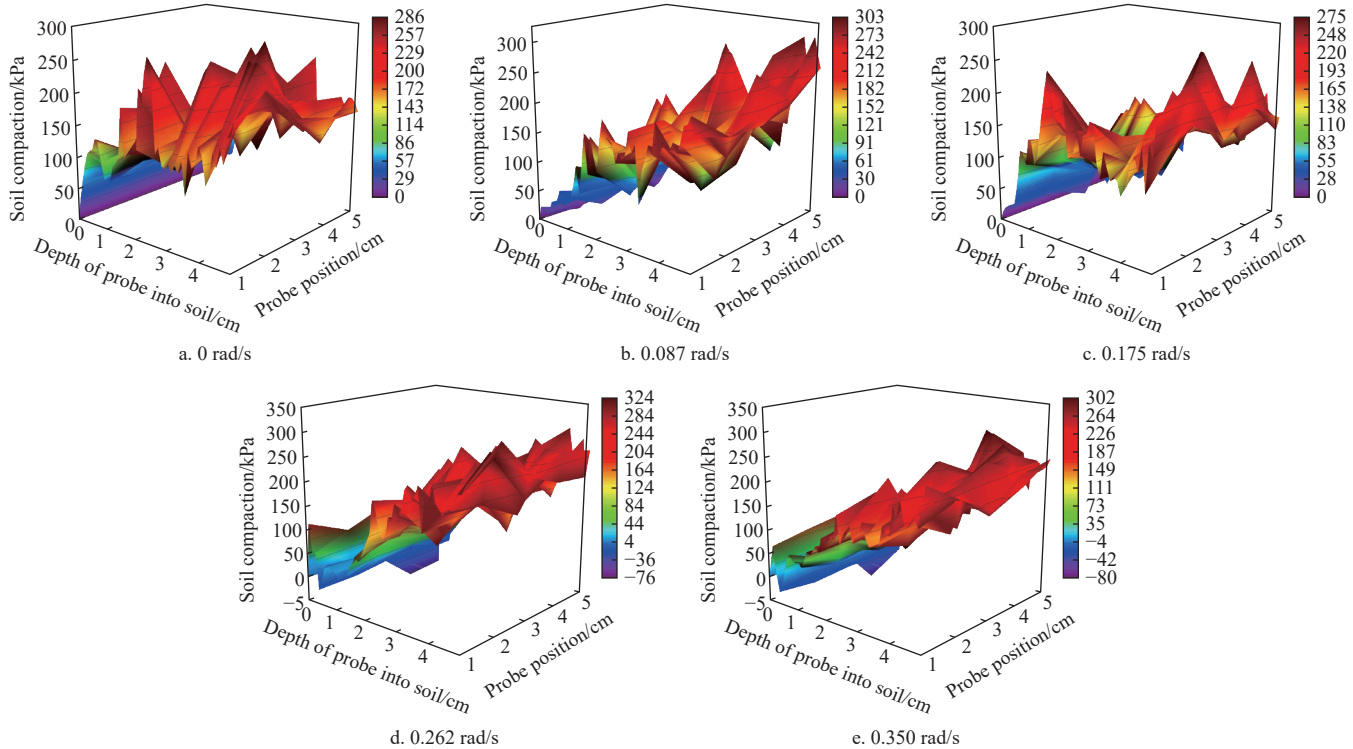

Figure 7 Soil compaction variation after SACCD operation under different real-time slope variation rates

3.4 Analysis and discussion of test results

As shown in Figure 3, the SACCD's operational performance was validated through field trials. In Lishu County, Siping City, Jilin Province, the measured CVSC was 20.4%, with an average soil

compaction of 194 kPa at 0-0.05 m depth and a seeding depth coefficient of variation of 9.6%. In Keshan County, Qiqihar City, Heilongjiang Province, the measured CVSC was 18.9%, soil compaction was 223 kPa, and seeding depth variation was 7.9%. The CVSC and seeding depth variation in Lishu were 1.5% and 1.7% higher, respectively, than those in Keshan. This is mainly due to greater slope variability and surface residue in Lishu, which increased the difficulty of residue removal and compromised profiling performance. In contrast, Keshan had lower slope variability and implemented effective residue management, resulting in minimal impact on SACCD performance. In both locations, the SACCD met operational quality requirements[14].

In Lishu, the maximum slope change over 5 meters reached approximately 12.5°, corresponding to an average slope variation rate of 0.087 rad/s. The field CVSC was 8.32% higher than in the simulations, and soil compaction error at 0-0.05 m depth was 9%. In Keshan, slope variation was negligible (0 rad/s), with a CVSC error of 1.02% and soil compaction error of 15% compared to the simulations. The larger compaction error in Keshan is attributable to the simulation model being calibrated based on Lishu's soil properties. Keshan's higher soil moisture content and cohesiveness contributed to increased soil compaction[32]. Nonetheless, the SACCD's operational stability remained robust. The consistency between simulation and field results confirms the accuracy of the model. During field operations, camera footage captured the SACCD's response to terrain fluctuations (Figure 3l), which closely mirrored the simulated profiling movements (Figure 3d). The soil particles were observed to be displaced toward the center and rear of the compacting wheels (Figure 3f), in line with simulated behavior. During field operations, the soil in Keshan exhibited higher moisture content and was relatively cohesive, making it difficult for the covering-compacting wheels of the SACCD to displace soil particles (Figure 3l). This observation was consistent with the simulation results (Figure 3d). However, at the Lishu test site, where the soil moisture content was lower, soil particles were more easily lifted by the covering-compacting wheels under load (Figure 3m), showing some deviation from the simulated results. Nonetheless, the overall effectiveness of soil covering and compaction in the field remained largely consistent with the simulation outcomes. These findings align with the patterns of soil particle behaviour during compaction operations reported by Zhao et al.[18] and Zhang et al.[13].

4 Conclusions

This study developed a DEM–MBD coupled simulation model to analyze the operation of a slope-adaptive covering–compacting device (SACCD) under dynamic slope variation conditions. The model effectively captured the system's key mechanical behaviors, demonstrating that increasing slope variation rates lead to asynchronous left–right wheel responses due to their different tilt tendencies. Response surface optimization provided the optimal structural parameters, and field experiments confirmed the accuracy of the model and the rationality of the SACCD design. The profiling posture, compaction force trends, and soil responses observed in the field showed strong agreement with simulation results, indicating that the model can reliably predict SACCD performance across different sloped-farmland scenarios.

Although the model performed well, future work could integrate more diverse soil conditions, incorporate real-time sensing and closed-loop control, and extend the modeling framework to multi-row or multi-component systems. These efforts would further enhance the applicability of slope-adaptive soil-covering and compaction technologies in complex terrain environments.

Acknowledgements

This work was supported by the National Key R&D Program of China [2022YFD1500704-1].

[References]

[1] Liu B Y, Xie Y, Li Z G, Liang Y, Zhang W B, Fu S H, et al. The assessment of soil loss by water erosion in China. International Soil and Water Conservation Research, 2020; 8(4): 430–439.

[2] Ren L D, Vanden Nest T, Ruysschaert G, D'Hose T, Cornelis W M. Short-term effects of cover crops and tillage methods on soil physical properties and maize growth in a sandy loam soil. Soil & Tillage Research, 2019; 192: 76–86.

[3] Zhang M J, Zhang W, Zhang K L, Yu Y, Liu L. Centennial scale temporal responses of soil magnetic susceptibility and spatial variation to human cultivation on hillslopes in Northeast China. Soil & Tillage Research, 2023; 234: 105865.

[4] Júnnyor W d S G, De Maria I C, Araujo-Junior C F, Diserens E, Severiano E d C, Farhate C V V, et al. Conservation systems change soil resistance to compaction caused by mechanised harvesting. Industrial Crops and Products, 2022; 177: 114532.

[5] Zhang H, He H L, Gao Y J, Mady A, Filipovic V, Dyck M, et al. Applications of Computed Tomography (CT) in environmental soil and plant sciences. Soil & Tillage Research, 2023; 226: 105574.

[6] Afzalinia S, Zabihi J. Soil compaction variation during corn growing season under conservation tillage. Soil & Tillage Research, 2014; 137: 1–6.

[7] Altikat S, Celik A. The effects of tillage and intra-row compaction on seedbed properties and red lentil emergence under dry land conditions. Soil & Tillage Research, 2011; 114(1): 1–8.

[8] Berti M T, Johnson B L, Henson R A. Seeding depth and soil packing affect pure live seed emergence of cuphea. Industrial Crops and Products, 2008; 27(3): 272–278.

[9] Chen G H, Weil R R, Hill R L. Effects of compaction and cover crops on soil least limiting water range and air permeability. Soil & Tillage Research, 2014; 136: 61–69.

[10] Sharipov G M, Paraforos D S, Griepentrog H W. Modelling and simulation of the dynamic performance of a no-till seeding assembly with a semi-active damper. Computers and Electronics in Agriculture, 2017; 139: 187–197.

[11] Sharipov G M, Paraforos D S, Griepentrog H W. Implementation of a magnetorheological damper on a no-till seeding assembly for optimising seeding depth. Computers and Electronics in Agriculture, 2018; 150: 465–475.

[12] Cao X P, Wang Q J, Li H W, He J, Lu C Y, Xu D J, et al. Design and experiment of the pneumatic pressure control device for no-till planter. Int J Agric & Biol Eng, 2023; 16(3): 37–46.

[13] Zhang C L, Wang X G, Guo M Z, Zhao J L, Li M J. A compacting device of rice dry direct-seeding planter based on DEM-MFBD coupling simulation significantly improves the seedbed uniformity and seedling emergence rate. Biosystems Engineering, 2024; 246: 26–40.

[14] Jia H L, Wang W J, Luo X F, Zheng J X, Guo M Z, Zhuang J. Effects of profiling elastic press roller on seedbed properties and soybean emergence under double row ridge cultivation. Soil & Tillage Research, 2016; 162: 34–40.

[15] Xie D B, He J X, Liu T, Liu C, Zhao G, Chen L Q. Establishment and validation the DEM-MBD coupling model of flexible straw-Shajiang black soil-walking mechanism interactions. Computers and Electronics in Agriculture, 2024; 224: 109203.

[16] Zhao Z, Li H C, Liu J K, Yang S X. Control method of seedbed compactness based on fragment soil compaction dynamic characteristics. Soil & Tillage Research, 2020; 198: 104551.

[17] Li B, Chen Y, Chen J. Modeling of soil-claw interaction using the discrete element method (DEM). Soil & Tillage Research, 2016; 158: 177–185.

[18] Zhao H B, Li H W, Ma S C, He J, Wang Q J, Lu C Y, et al. The effect of various edge-curve types of plain-straight blades for strip tillage seeding on torque and soil disturbance using DEM. Soil & Tillage Research, 2020; 202: 104674.

[19] Horabik J, Molenda M. Parameters and contact models for DEM

simulations of agricultural granular materials: A review. Biosystems Engineering, 2016; 147: 206–225.

[20] Mudarisov S, Farkhutdinov I, Khamaletdinov R, Khasanov E, Mukhametdinov A. Evaluation of the significance of the contact model particle parameters in the modelling of wet soils by the discrete element method. Soil & Tillage Research, 2022; 215: 105228.

[21] Deng H, Dai F, Shi R J, Song X F, Zhao W Y, Pan H F. Simulation of full-film double-row furrow roller hole fertiliser application based on DEM-MBD coupling and research on its water and fertiliser transport law. Biosystems Engineering, 2024; 239: 190–206.

[22] Liu B W, Zhou Z Y, Gan J Q, Ellis D, Zou R P, Yu A B. Investigation of performance of hydraulic excavators by co-simulation of multibody dynamics and discrete element method. Powder Technology, 2023; 414: 118088.

[23] Chen G B, Wang Q J, Li H W, He J, Wang X H, Zhang X Y, et al. Experimental research on vertical straw cleaning and soil tillage device based on Soil-Straw composite model. Computers and Electronics in Agriculture, 2024; 216: 108510.

[24] Fang W Q, Wang X Z, Han D L, Zang N, Chen X G, Ohiemi I E. Parameter optimization and disturbance analysis of the film picking device of the chain-type plough layer residual film recovery machine based on DEM-MBD coupling. Computers and Electronics in Agriculture, 2024; 222: 109041.

[25] Zhang B, Wang J Y, Yang X S, Chen B S. A DEM-MBD based method for regulating transfer flux in the supply and discharge of cane seed particles. Computers and Electronics in Agriculture, 2024; 218: 108732.

[26] Li H, He J, Wang Q J, Wang C, Wu Z Y, Guo Z Y. Analysis of slope-adaptive in covering-compacting device for no-till sowing based on DEM-MBD. Computers and Electronics in Agriculture, 2025; 233: 110175.

[27] Chen G B, Wang Q J, Li H W, He J, Lu C Y, Xu D J, et al. Experimental research on a propeller blade fertilizer transport device based on a discrete element fertilizer block model. Computers and Electronics in Agriculture, 2023; 208: 107781.

[28] Ucgul M, Saunders C, Li P, Lee S H. Analysing the mixing performance of a rotary spader using digital image processing and discrete element modelling (DEM). Computers and Electronics in Agriculture, 2018; 151: 1–10.

[29] Wu Z Y, Wang X S, Liu D W, Xie F P, Ashwehmbom L G, Zhang Z Z, et al. Calibration of discrete element parameters and experimental verification for modelling subsurface soils. Biosystems Engineering, 2021; 212: 215–227.

[30] Sun J L, Yang L, Zhang D X, Hu J Y, Cui T, He X T, et al. Development of a prediction model to determine optimal sowing depth to improve maize seedling performance. Biosystems Engineering, 2023; 234: 206–222.

[31] Vasu D, Singh S K, Sahu N, Tiwary P, Chandran P, Duraisami V P, et al. Assessment of spatial variability of soil properties using geospatial techniques for farm level nutrient management. Soil & Tillage Research, 2017; 169: 25–34.

[32] Yang S R, Lin H D, Huang W H. Variation of initial soil suction with compaction conditions for clayey soils. Journal of Mechanics, 2012; 28(3): 431–437.